

# Nanoscale

Accepted Manuscript



This is an *Accepted Manuscript*, which has been through the Royal Society of Chemistry peer review process and has been accepted for publication.

*Accepted Manuscripts* are published online shortly after acceptance, before technical editing, formatting and proof reading. Using this free service, authors can make their results available to the community, in citable form, before we publish the edited article. We will replace this *Accepted Manuscript* with the edited and formatted *Advance Article* as soon as it is available.

You can find more information about *Accepted Manuscripts* in the [Information for Authors](#).

Please note that technical editing may introduce minor changes to the text and/or graphics, which may alter content. The journal's standard [Terms & Conditions](#) and the [Ethical guidelines](#) still apply. In no event shall the Royal Society of Chemistry be held responsible for any errors or omissions in this *Accepted Manuscript* or any consequences arising from the use of any information it contains.

# Absolute photoluminescence quantum yields of IR26 and IR-emissive $\text{Cd}_{1-x}\text{Hg}_x\text{Te}$ and PbS quantum dots – Method- and material-inherent challenges

*Soheil Hatami<sup>a</sup>, Christian Würth<sup>a</sup>, Martin Kaiser<sup>a</sup>, Susanne Leubner<sup>b</sup>, Stefanie Gabriel<sup>b</sup>, Lydia Bahrig<sup>b</sup>, Vladimir Lesnyak<sup>b,c</sup>, Jutta Pauli<sup>a</sup>, Nikolai Gaponik<sup>b</sup>, Alexander Eychmüller<sup>b</sup>, Ute Resch-Genger<sup>a\*</sup>*

<sup>a</sup> BAM Federal Institute for Materials Research and Testing, Richard-Willstaetter-Str. 11, 12489 Berlin, Germany

<sup>b</sup> Physical Chemistry and Center for Advancing Electronics Dresden, TU Dresden, Bergstr. 66b, 01062 Dresden, Germany

<sup>c</sup> Department of Nanochemistry, Istituto Italiano di Tecnologia, via Morego, 30, 16163 Genova, Italy

\* Email: [ute.resch@bam.de](mailto:ute.resch@bam.de)

## Abstract

Bright emitters with photoluminescence in the spectral region of 800 – 1600 nm are increasingly important as optical reporters for molecular imaging, sensing, and telecommunication and as active components in electrooptical and photovoltaic devices. Their rational design is directly linked to suitable methods for the characterization of their

signal-relevant properties, especially their photoluminescence quantum yield ( $\Phi_f$ ). Aiming at the development of bright semiconductor nanocrystals with emission  $> 1000$  nm, we designed a new NIR/IR integrating sphere setup for the wavelength region of 600 – 1600 nm. We assessed the performance of this setup by acquiring the corrected emission spectra and  $\Phi_f$  of the organic dyes Itrybe, IR140, and IR26 and several infrared (IR)-emissive  $\text{Cd}_{1-x}\text{Hg}_x\text{Te}$  and PbS semiconductor nanocrystals and comparing them to data obtained with two independently calibrated fluorescence instruments absolutely or relatively to previously evaluated reference dyes. Our results highlight special challenges of photoluminescence studies in the IR ranging from solvent absorption to the lack of spectral and intensity standards together with quantum dot-specific challenges like photobrightening and photodarkening and the size-dependent air stability and photostability of differently sized oleate-capped PbS colloids. These effects can be representative for lead chalcogenides. Moreover, we redetermined the  $\Phi_f$  of IR26, the most frequently used IR reference dye, to  $1.1 \times 10^{-3}$  in 1,2-dichloroethane DCE with a thorough sample reabsorption and solvent absorption correction. Our results indicate the need for a critical reevaluation of  $\Phi_f$  values of IR-emissive nanomaterials and offer guidelines for improved  $\Phi_f$  measurements.

### Keywords

Fluorescence; dye; quantum dot; absolute quantum yield; integrating sphere; NIR; IR; cyanine; IR140; IR26; PbS; CdHgTe; photobrightening; stability; surface modification

## 1 Introduction

Fundamental advances in biochemical assays, molecular sensors, optical imaging, telecommunication, and optical, electroluminescent, and photovoltaic devices require bright and stable fluorophores.<sup>1-7</sup> A straightforward measure for fluorophore performance presents the photoluminescence quantum yield ( $\Phi_f$ ),<sup>8, 9</sup> given by the number of emitted photons  $N_{em}$  per number of photons  $N_{abs}$  absorbed by the system, see equation 1.<sup>9-11</sup> For fluorescent nanomaterials like semiconductor nanocrystals (NC), i.e., quantum dots and rods,<sup>8</sup> and for upconversion nanocrystals (NCs),<sup>12, 13</sup> where surface states and the accessibility of emissive states by quenchers largely control accomplishable  $\Phi_f$  values,<sup>14-18</sup> the value of  $\Phi_f$  provides also a straightforward tool to assess the quality of the surface shell and surface passivation and hence, to evaluate new synthetic and surface functionalization strategies.<sup>19</sup> Moreover, concentration-dependent  $\Phi_f$  give a direct hint for ligand desorption as recently shown for e.g., CdTe and CdSe quantum dots,<sup>14, 15, 20-22</sup> which is typically the first step to material decomposition, resulting in the release of toxic heavy metal ions.<sup>8, 20, 23</sup>

$$\Phi_f = \frac{N_{em}(\lambda)}{N_{abs}(\lambda)} \quad (\text{eq. 1})$$

$\Phi_f$  can be obtained directly with optical methods either relative to a fluorescent reference with known  $\Phi_f$  or as absolute quantity (standard-free),<sup>9, 11, 24, 25</sup> or with calorimetric methods like photoacoustic spectroscopy and thermal lensing.<sup>26-28</sup> Commonly,  $\Phi_f$  is obtained optically, comparing the absorption-weighted integral fluorescence intensities of a sample and a reference measured under identical conditions.<sup>9, 11, 24</sup> Due to the need of standards with reliably known  $\Phi_f$ , this

straightforward procedure is limited predominantly to the ultraviolet (UV), visible (vis) and NIR region, where  $\Phi_f$  standards have been recommended for many years<sup>9, 24, 25, 27-32</sup> or recently provided by us.<sup>9, 25</sup> This included the reevaluation of  $\Phi_f$  of IR125 in dimethylsulfoxide (DMSO), the most frequently used NIR reference dye for organic fluorophores and semiconductor NCs,<sup>33-37</sup> yielding a  $\Phi_f$  of 0.23<sup>9</sup> instead of the previously assumed  $\Phi_f$  of 0.13,<sup>38</sup> and consequently, an underestimation of all  $\Phi_f$  values obtained relatively to this dye. Nevertheless, the accurate determination of  $\Phi_f > 1000$  nm still presents a considerable challenge as indicated by the recently reexamined  $\Phi_f$  of the most frequently used IR  $\Phi_f$  reference dye IR26,<sup>39-42</sup> demonstrating large deviations in its  $\Phi_f$  in 1,2-dichloroethane (DCE) by a factor of up to 10.<sup>43-45</sup> This was recently addressed in depth by absolute measurements of its  $\Phi_f$  by Semonin et al. using a self-made integrating sphere setup.<sup>43</sup> These high uncertainties in the red wavelength region originate from the fact that many critical issues affecting especially photoluminescence measurements in the IR wavelength region like the performance and validation of instrument calibrations,<sup>46</sup> solvent and water vapor absorption, and sample reabsorption,<sup>24, 47, 48</sup> have not been really detailed yet. Moreover, semiconductor NC-specific effects like material- and surface chemistry-dependent photodecomposition and photobrightening,<sup>8, 14, 49</sup> that can depend on the incident spectral radiant flux and even on NC size, or a possible excitation wavelength dependence of  $\Phi_f$ <sup>50, 51</sup> were not addressed.

Aiming at the rational design of bright NIR- and IR-emissive SCNCs with emission in the wavelength region of 650 – 1600 nm and to address the relevance of the reliable characterization of emerging luminescent reporters for the NIR II window of 1000 – 1700 nm for e.g., bioimaging studies,<sup>52-54</sup> we present the design of a new integrating sphere

setup for absolute measurements of photoluminescence spectra and  $\Phi_f$  from 600 – 1600 nm and its calibration and performance validation. Subsequently, we reexamined  $\Phi_f$  of IR26 and quantified measurement uncertainties. Then, we measured  $\Phi_f$  of representative NIR- and IR-emissive semiconductor NCs, here  $\text{Cd}_{1-x}\text{Hg}_x\text{Te}$  colloids with size- and composition tuning of the optical and electrochemical properties,<sup>42, 55, 56</sup> and differently sized PbS, presenting the most commonly used NCs in photovoltaics,<sup>3, 33, 57</sup> to provide examples for achievable  $\Phi_f$  values.

## 2 Methods

### 2.1 Reagents and materials

The  $\Phi_f$  standards HITCI (batch number 029006) and IR 125 (batch number 10970) used for relative measurements, and IR 140 (batch number 9310) were obtained from Lambda Physics, the spectral emission standard Itrybe from Otava (batch number OTVD\_0037), and IR 26 from Acros (batch number 409401000), respectively. The chemical structures are given in the SI (Figure 1S). The solvents used for the spectroscopic studies, i.e., ethanol for Itrybe and HITCI, dimethylsulfoxide (DMSO) for IR125 and IR140, 1,2-dichloroethane (DCE) for IR26, and tetrachloroethylene (TCE) for PbS, respectively, were of spectroscopic grade and purchased from Sigma Aldrich and Merck. For  $\text{Cd}_{1-x}\text{Hg}_x\text{Te}$ , deuterated water ( $\text{D}_2\text{O}$ ) from Merck was employed.

### 2.2 Synthesis of semiconductor NCs

$\text{Cd}_{1-x}\text{Hg}_x\text{Te}$  of different composition and size were synthesized in water as previously described using mercaptopropionic acid (MPA) as ligand<sup>42</sup> and stored in the dark in air.

Differently sized PbS colloids were prepared according to Poppe et al.<sup>58</sup> under inert gas, purified, and stored as stock solutions in toluene either in a glove box or under inert gas atmosphere or in air in the dark in the refrigerator.

### 2.3 Characterization

Dye purity was determined by high performance liquid chromatography (HPLC) with the Agilent 1200 HPLC system (Agilent) using a previously reported method<sup>25</sup> and yielded the following purities (100 % method): HITCI: 97.9 % (760 nm),<sup>25</sup> IR125: 99.1 % (800 nm),<sup>25</sup> Itrybe: 99.8 % (600 nm), IR 140: 90.2 % (700 nm), and IR 26: 99.5 % (750 nm). The size of the PbS NCs was obtained from absorption spectra to 2.3 nm, 4.1 nm, and 4.4 nm, respectively, as described by Catemartiri et al.<sup>59</sup> The size and composition of the Cd<sub>1-x</sub>Hg<sub>x</sub>Te NCs was determined to 4.8 nm, 6.3 nm, and 7.1 nm for colloids with Cd:Hg ratios of 99:1, 98:2, and 97:3, respectively, using TEM and ICP-OES. Absorption spectra were recorded on a calibrated Cary 5000 spectrometer. Fluorescence emission spectra and  $\Phi_f$  were measured with a FSP920 spectrofluorometer (Edinburgh Instruments; 300 – 1700 nm; relative measurements with HITCI ( $\Phi_f = 0.30$ ; ethanol) and IR 125 ( $\Phi_f = 0.23$ ; DMSO) as references),<sup>9, 24, 25</sup> a custom made UV/vis/NIR integrating sphere setup (350 – 1050 nm),<sup>25</sup> and our newly designed NIR/IR integrating sphere setup (600 – 1600 nm), respectively, all independently calibrated (see *Supporting Information (SI)* for details on instrumentation and calibration including transfer standards employed). All absorption and fluorescence measurements were performed with freshly prepared dye or NC solutions (absorbances A of 0.02 to 0.1 at the longest wavelength absorption maximum or first excitonic peak) at T = (25 ± 1)°C in air using either 10 mm×10 mm quartz cuvettes

from Hellma GmbH or 10 mm × 4 mm cells to minimize dye or NC reabsorption and/or solvent absorption. For IR26, absorbances of up to 0.8 were used. Stock solutions of Cd<sub>1-x</sub>Hg<sub>x</sub>Te NC stored in air in the dark at room temperature were diluted with D<sub>2</sub>O by a factor of at least 1000:1 before each measurement. For potentially air-sensitive PbS colloids, aging studies were performed with the stock solutions of the three PbS colloids in toluene, stored in air in the dark in the refrigerator. To representatively address the influence of oxygen, the 4.4 nm-sized PbS NC batch was split into two portions, one being kept always under inert gas in the dark at room temperature and the other one under identical conditions as the stock solutions of the smaller PbS colloids. For the spectroscopic studies, the PbS stock solutions were always diluted by a factor of at least 1000:1 with TCE and measured in air, except for 4.4 nm PbS stored and aged under inert gas. In this case, TCE dilution was performed in a glove box and sealed cells were used for subsequent spectroscopic measurements. All fluorescence emission spectra shown were blank-corrected and corrected for instrument-specific effects relative to the spectral photon radiance scale.<sup>46, 60, 61</sup> Relative standard deviations of fluorescence measurements were obtained from four independent measurements. Spectra correction such as a reabsorption correction<sup>9, 24, 25</sup> and solvent absorption correction are detailed in the *SI*.

### 3 Results and Discussion

#### 3.1 Design of an integrating sphere setup for the NIR and IR

The design of our integrating sphere setup for absolute  $\Phi_f$  measurements from 600 – 1600 nm with versatile excitation, reasonable spectral resolution, and high sensitivity is shown in Figure 1 (for more details on setup components, see *SI*). To optimize the



sensitivity of the setup, which should enable not only the determination of the moderate to high  $\Phi_f$  of semiconductor NC exceeding 0.1, yet also of organic dyes with emission > 1000 nm like IR26 with very small  $\Phi_f < 5 \times 10^{-3}$ ,<sup>43</sup> we chose a small integrating sphere (diameter of *ca.* 11 cm) with a high reflectivity hydrophobic Spectralon coating (99 % from 400 – 1500 nm) as sample compartment, thereby minimizing water adsorption from air. This sphere, which is large enough to minimize distortions of the radiating field in the sphere by the sample, was equipped with six ports for sample illumination, positioning of the sample holder, emission detection, and purging with dry nitrogen to remove water vapor absorbing at around 950 nm, 1130 nm, and 1450 nm (see *SI*, Figure 7S). This avoids distortions of the measured transmitted excitation light and photoluminescence, that become otherwise dependent on air humidity (and ambient temperature) and optical path length. As excitation light sources, we chose different high stability (intensity fluctuations < 1 %; see *SI*) intense lasers (HeNe laser: 633 nm), laser diodes (690 nm, 730 nm, 785 nm, 808 nm, and 980 nm), and a diode-pumped solid-state laser (914 nm), respectively, to enable the measurement of dye and NC samples absorbing and emitting over a broad wavelength region with strongly varying photoluminescence efficiencies. These light sources were coupled via fiber optics (Figure 1, top) to the integrating sphere (Figure 1, bottom) or directed either directly into the middle of the sphere (sample position) or on the sphere wall with a flat mirror. This enables direct and indirect sample illumination and their combination.<sup>62</sup> The small spot diameters of 1-4 mm of these excitation light sources provide control of the illuminated volume to minimize solvent absorption and reabsorption effects. This is of special relevance for measurements of solutions and dispersions > 950 nm due to the absorbance of many solvents and matrices

in this wavelength region (Figure 3, right panel). For signal detection, we used an imaging spectrograph attached to a Peltier cooled, thinned back side illuminated deep depletion InGaAs CCD with high quantum efficiencies of > 85 % (1100 – 1500 nm). The N<sub>2</sub>-purged spectrograph-detector ensemble was coupled to the integrating sphere with an IR-suitable quartz fiber bundle (LLB552-IR-0,12, IR Quartz, LOT Oriel, Transmission > 50 %) shielded from direct reflexes with several baffles. We placed a filter wheel with neutral density (ND) filters (known wavelength-dependent transmission) in front of the integrating sphere for control and variation of the incident radiant power and a filter wheel with several long pass (LP) interference filters (cut-on wavelengths of 600 nm, 800 nm, 950 nm, and 1000 nm) in front of the spectrograph-CCD ensemble to eliminate signal distorting second order diffractions and stray light . Dye solutions and NC dispersions in quartz cells were center-mounted in the sphere with a custom designed Spectrafect-coated cuvette holder positioned with a HeNe-laser.

*<Insert Figure 1 here>*

### **3.2 Setup characterization**

We subsequently determined the wavelength accuracy of the excitation and detection channel(s), the linearity of the detection channel, and the wavelength-dependent spectral responsivity of the integrating sphere-spectrograph-CCD ensemble ( $s(\lambda_{em})$ )<sup>46</sup>. The wavelength accuracy of the emission monochromator revealed maximum deviations < 1.1 nm (see *SI*, Figure 3S). Relative deviations from a linear behavior of the InGaAs CCD measured at a constant integration time for varying excitation radiant powers amounted to 0.3 % (see *SI*, Figure 4S) and for a constant radiant power and varying integration times

to 0.5 %, respectively. To reduce calibration uncertainties in  $s(\lambda_{em})$  caused by stray light and second order effects and account for the lack of suitable emission standards  $> 950$  nm, we employed two calibration lamps, a conventional spectral radiance transfer standard (SDS)<sup>63</sup> with an emission maximum at 1050 nm and a blackbody radiator (BBR) with a temperature-controlled spectral radiance, with an emission maximum at 1970 nm (for  $T = 1200$  °C). An example for an emission correction curve (equaling  $1/s(\lambda_{em})$ ) derived from the combination of these measurements (see *SI*, Figure 6S) is shown in Figure 2 (top panel; SDS: emission correction curve for 600 – 950 nm; BBR: emission correction curve measured for 950 – 1600 nm). The relative uncertainty for the determination of  $s(\lambda_{em})$  from such combined calibration curves amounts to maximum 12 %. This value includes uncertainties of the certified values of the calibrated light sources, the wavelength accuracy, linearity of the detection system, contributions from stray light, specific uncertainties arising from the different types of light sources and merging of the emission correction curves. Finally, the long term stability of the spectral radiant power of the different light sources of the integrating sphere setup was obtained as this is a critical parameter for all absolute measurements of  $\Phi_f$ .<sup>25</sup> Multiple measurements over time using typical measurement conditions (integration time, number of accumulations; see *SI*, Figure 5S for exemplarily light sources) revealed relative deviations of the mean values (integration over the entire excitation peak) of  $< 1$  %.

### 3.3 Setup validation - Comparison of emission spectra

Proper validation of the calibration of the wavelength and intensity scale is the only way to reliable emission spectra and  $\Phi_f$  values. The good agreement between the emission

correction curves obtained with SDS and BBR (see *SI*, Figure 6S) provides already a first hint for the accuracy of our emission correction curve. For control of  $s(\lambda_{em})$  in the wavelength region of 600 – 1000 nm, we acquired the corrected emission spectra of the NIR dyes Itrybe and IR140 in ethanol and DMSO, respectively, and for 900 – 1600 nm the corrected emission spectra of different IR-emissive semiconductor NCs, here mercaptopropionic acid (MPA)-stabilized  $Cd_{1-x}Hg_xTe$  NCs of various composition and size dispersed in  $D_2O$  and PbS colloids of various size in TCE with the NIR/IR sphere setup and our independently calibrated fluorometer. The generally good match between these emission spectra (Figure 2, middle panel), indicated by the small relative spectral deviations in the order of typically 5 % (Figure 2, lower panel) underlines the reliability of our emission correction curve.

*<Insert Figure 2 here>*

### 3.4 Fluorescence quantum yields of NIR dyes with emission < 1000 nm

Subsequently, we measured  $\Phi_f$  of the NIR dyes Itrybe (solvent ethanol; emission: 680 – 950 nm;  $\lambda_{ex} = 633$  nm)<sup>64</sup> and IR140 (solvent DMSO; emission: 830 – 1050 nm;  $\lambda_{ex} = 808$  nm) with our NIR/IR and/or UV/vis/NIR integrating sphere setups and our calibrated fluorometer FSP920. Itrybe and IR140 were chosen because of their different Stokes shifts providing examples for small (Itrybe)<sup>64</sup> and large (IR140) spectral overlap between absorption and emission and their commercial availability in high purity as well as their subsequently derived good photochemical stability (see *SI*, Figure 9S) and their excitation

wavelength-independent  $\Phi_f$ . The good agreement between underlines the reliability of  $\Phi_f$  measurements with our new integrating sphere in the wavelength region of 630 – 1050 nm. We previously provided an uncertainty budget for  $\Phi_f$  measurements in the wavelength region of 400 – 1000 nm.<sup>9, 24, 25</sup>

*<Insert Table 1 here>*

### 3.5 Reassessment of $\Phi_f$ of IR 26 with emission > 1000 nm

For control of the reliability of  $\Phi_f$  measurements > 1000 nm, we chose IR26 in DCE (excitation range: 800 – 1000 nm, emission: 1010 – 1450 nm; see Figure 3, left panel). Together with IR125 in DMSO, this dye presents the most common reference for red emissive NCs. Moreover, its  $\Phi_f$  was only recently redetermined absolutely to  $4.8 \times 10^{-4}$ ,<sup>43</sup> which is by a factor of *ca.* 10 lower than previously assumed,<sup>44, 45</sup> rendering all  $\Phi_f$  measured relative to this dye questionable.<sup>39, 40, 42</sup> Its extremely low  $\Phi_f$  enables also to test the sensitivity of our new setup. Other challenges of the measurement of  $\Phi_f$  of IR26 presented the strong spectral overlap between its absorption and emission bands favoring reabsorption and the absorption of the recommended solvent DCE within the dye's emission band with a sharp maximum at *ca.* 1170 nm (Figure 3, left and right panel). Solvent absorption occurs for many common solvents > 900 nm (Figure 3, right), hence, uncertainties of determined quantum yields in this wavelength region exceed those of measurements at smaller wavelengths. Solvent and reabsorption effects are especially critical for integrating sphere measurements, as the size of the resulting signal distortions

depends on sphere diameter and reflectivity of the sphere coating as well as on the sample volume.

*<Insert Figure 3 here>*

We determined the  $\Phi_f$  of IR26 in DCE (see Table 1) absolutely at dye concentrations of  $0.7 \times 10^{-6}$  to  $6 \times 10^{-6}$  mol/L (equaling absorbances of 0.09 – 0.80 at the absorption maximum of 1082 nm using a molar absorption coefficient  $\varepsilon = 1.4 \times 10^{-5}$  Lmol<sup>-1</sup>cm<sup>-1</sup> <sup>65</sup>) and with our spectrofluorometer relative to IR125 in DMSO<sup>9, 25</sup> (IR26:  $\lambda_{\text{ex}} = 980$  nm; IR125:  $\lambda_{\text{ex}} = 808$  nm; see *SI*, Figure 2S).<sup>24, 46</sup> Absorption spectra of these dye solutions revealed the absence of dye aggregates at these concentrations (see *SI*, Figure 8S) and the photochemical stability of IR26 was sufficient for excitation with a 980 nm laser diode (see *SI*, Figure 9S). The sharp dip in the measured emission band of IR26 at *ca.* 1170 nm shown in Figure 3 (left panel, red spectrum) demonstrates the considerable influence of solvent absorption. The influence of dye reabsorption on IR26 fluorescence follows from the red shift and reduced intensity of the as measured emission band compared to the reabsorption- and solvent-absorption-corrected fluorescence spectrum (Figure 3, left panel, black spectrum). This is reflected by the corresponding  $\Phi_f$  data, i.e., a  $\Phi_f$  of  $0.7 \times 10^{-3}$  as measured, which amounts to  $1.1 \times 10^{-3}$  after consideration of solvent absorption and dye reabsorption (see *SI*; Figure 8S).<sup>9, 24, 25</sup> We determined the relative uncertainty of this value to 21 % ( $2.3 \times 10^{-4}$ ). This includes contributions from setup calibration (12 %) and applied corrections (15 %) as well as the relative standard deviation of fluorescence measurements with our NIR/IR integrating sphere setup (9 %). Relative measurements

yielded  $\Phi_f$  of  $0.7 \times 10^{-3}$  (Table 1). We estimated the relative uncertainty of this value to 30 % ( $2.1 \times 10^{-4}$ ) taking into account uncertainties from instrument calibration (emission correction from instrument manufacturer, two point self-made excitation correction,  $\Phi_f$  uncertainty of the reference dye IR125), dye reabsorption and solvent absorption and the relative standard deviation of fluorescence measurements. Dye purity was not considered in both cases.

We attribute our finding of a higher  $\Phi_f$  for IR26 as the value of  $0.48 \times 10^{-3}$  reported by Semonin et al.<sup>43</sup> to different calibration and correction procedures. Nevertheless, our value still equals the absolute upper limit of  $\Phi_f$  of this dye assumed by Semonin. In addition, the fact that we could measure  $\Phi_f$  absolutely at concentrations of  $0.7 \times 10^{-6}$  to  $6 \times 10^{-6}$  mol/L demonstrates the higher sensitivity of our integrating sphere setup compared to the setup reported by Semonin et al. who used dye concentrations of  $2 \times 10^{-6}$  to  $11 \times 10^{-6}$  mol/L (equaling absorbances of 0.3 – 1.5 at the absorption maximum of 1082 nm) for the integration sphere measurement of  $\Phi_f$  of IR26. In this respect, the measurement uncertainties given by us for the absolute determination of  $\Phi_f$  of IR26 exceed only apparently the uncertainty provided by Semonin et al. of  $0.2 \times 10^{-4}$  (equaling a relative uncertainty of 4.2 %) that was not really deduced from the actual integrating sphere measurements. This uncertainty was derived by Semonin et al. only from a fit considering dye reabsorption, yet not solvent absorption, which was made for a  $0^\circ/90^\circ$  measurement geometry and not for the integrating sphere measurements. Most likely, the small uncertainties given by Semonin et al. consider solely the standard deviation of the fluorescence measurements, but not a complete uncertainty budget as given by us.<sup>24, 25</sup>

Nevertheless, our data verify the considerable overestimation of many  $\Phi_f$  of NIR- and IR-emissive NCs like PbS, PbSe, and Cd<sub>1-x</sub>Hg<sub>x</sub>Te.<sup>39, 40, 42</sup> This finding, together with the  $\Phi_f$  values absolutely measured for PbS in different solvents in the order of 0.05 to 0.60<sup>43, 66-68</sup> and relatively to IR125 (using a reference  $\Phi_f$  of 0.13)<sup>38</sup> in the order of 0.20 to 0.40,<sup>33, 35</sup> respectively, clearly demonstrates the need for a critical reexamination of  $\Phi_f$  values of representative IR-emissive semiconductor NCs.

### 3.6 $\Phi_f$ of IR-emissive semiconductor Cd<sub>1-x</sub>Hg<sub>x</sub>Te ternary alloys

Especially promising IR-emissive NCs are Cd<sub>1-x</sub>Hg<sub>x</sub>Te ternary alloys as well as PbS and PbSe.<sup>3, 33, 42, 55-57</sup> As PbSe NCs can be more prone to surface oxidation as PbS NCs,<sup>69-72</sup> we decided to evaluate only the  $\Phi_f$  of dispersions of representative Cd<sub>1-x</sub>Hg<sub>x</sub>Te ternary alloys of different composition and size and exemplarily differently sized PbS colloids detailed in the following section to provide examples for achievable  $\Phi_f$  values for IR-emissive quantum dots and to identify NC-specific challenges and sources of uncertainty.

We determined the  $\Phi_f$  of three MPA-capped Cd<sub>x</sub>Hg<sub>1-x</sub>Te NC samples with comparatively broad emission spectra in D<sub>2</sub>O spanning a wavelength region from *ca.* 750 – 1350 nm shown in Figure 2 and Figure 4 (inset) at different excitation wavelengths between 633 to 785 nm relatively and absolutely. Prior to these measurements, we measured time traces with our integrating sphere setup to exclude photodecomposition and photobrightening for excitation with intense laser diodes, the radiant flux of which considerably exceeding that of a xenon lamp monochromator ensemble used for relative photoluminescence measurements. Moreover,  $\Phi_f$  were determined relatively before and



after each absolute measurement. These studies did not reveal light-induced changes of the  $\text{Cd}_{1-x}\text{Hg}_x\text{Te}$  NC colloids.

*<Insert Figure 4 here>*

As follows from Figure 4, the absolutely and relatively determined  $\Phi_f$  of the three  $\text{Cd}_{1-x}\text{Hg}_x\text{Te}$  colloids agree reasonably well. We determined the relative uncertainties of absolutely measured  $\Phi_f$  to 16 %, considering uncertainty contributions of setup calibration (12 %) and applied reabsorption and stray light corrections (5 %; see *SI*) as well as of the relative standard deviation of fluorescence measurements with the NIR/IR integrating sphere setup (10 %). The uncertainties of relatively measured  $\Phi_f$  are estimated to 15 % (no excitation correction, only small absorption of  $\text{D}_2\text{O}$ , less pronounced reabsorption as found for IR26). None of the colloids studied showed a dependence of its  $\Phi_f$  on excitation wavelength within the uncertainties. The comparatively high  $\Phi_f$  between *ca.* 0.3 and 0.65 of our colloids underline the suitability of our simple one pot aqueous synthesis<sup>42</sup> for the preparation of bright  $\text{Cd}_x\text{Hg}_{1-x}\text{Te}$  NCs especially with the ligand MPA.<sup>73</sup> Whether the observed trend of a decrease in  $\Phi_f$  with increasing size and/or Hg content is really representative, possibly originating from a confinement reduction with increasing particle size and/or the introduction of an increasing number of crystal and surface defects with larger numbers of  $\text{Hg}^{2+}$  ions (with sizes exceeding that of  $\text{Cd}^{2+}$ ) favoring luminescence quenching, remains to be shown for a larger set of samples.

### 3.7 Aging studies and $\Phi_f$ of IR-emissive PbS colloids

Subsequently, we investigated the spectroscopic properties of three oleate-capped PbS colloids of different sizes, i.e., 2.3 nm, 4.1 nm, and 4.4 nm, in TCE which does not absorb within the wavelength region of NC emission (Figure 2 and Figure 3, right panel; *SI*, Figure 10S). To account for a possible influence of oxygen and hence, NC oxidation, which is manifested by a blue shift in absorption and emission and can depend on particle size,<sup>72</sup> the 4.4 nm-sized PbS colloid batch was split into two portions immediately after synthesis. One portion was kept always under inert gas and the other sample was stored in air.

*PbS aging.* Spectroscopic studies of our differently sized PbS colloids kept in air and dispersed in TCE revealed a blue shift of the absorption and emission maxima with time in conjunction with a considerable narrowing of the blue shifted absorption band and a reduction in emission bandwidth, i.e., FWHM (full width at half height of the maximum). This is exemplarily shown for 4.4 nm PbS NCs in Figure 5 (top panel and lower panels), the largest NC of this series, which underwent the most pronounced changes (see *SI*, Figure 11S). Here, the initial emission maximum located at 1380 nm shifted to 1265 nm over a period of *ca.* 250 days, accompanied by a considerable narrowing of the absorption band (Figure 5, lower panel, left; comparison of black and blue solid spectrum) and the emission band (Figure 5, lower panel, right; initial FWHM of 250 nm (0.165 eV) developing into FWHM of 150 nm (0.113 eV)), respectively. Simultaneously,  $\Phi_f$  increased from 0.24 to 0.45 within 250 days and remained then stable (Figure 5, top). These  $\Phi_f$  values lay at the upper end of the  $\Phi_f$  values reported by Semonin et al.,<sup>43</sup> underlining the good quality of our PbS NC. This is similarly true for the two smaller PbS NC samples that showed a higher stability to aging, as indicated by their smaller time-

dependent spectral shifts in absorption and emission and changes in FWHM (see *SI*, Figure 11S). The smallest 2.3 nm-sized PbS particles reached a stable state almost immediately after synthesis (FWHM = 0.178 eV, no time-dependent changes). We attribute this size-dependent stability of our three PbS colloids to similar effects as reported by Choi et al. for oleate-capped PbS nanoparticles.<sup>72</sup> They claimed a size-dependent shape transition from air stable ligand-passivated (111) facets-only octahedrons to (111)/(100) cubooctahedrons, with bare self-passivated (100) facets being prone to surface oxidation.<sup>72</sup> The latter is reflected by the strong aging-induced changes in the optical properties of especially the 4.4 nm PbS NCs (Figure 5) which can be attributed to surface etching. This leads to a decrease of the PbS core size and the formation of an oxidized layer (PbSO<sub>x</sub>) on the surface of the PbS NC as recently reported by e.g., Tang et al.<sup>74</sup> and Hardman et al.<sup>75</sup> in conjunction with a focusing of the NC size distribution, indicated by the narrowing of the absorption and emission bands, that is possibly accompanied by a shape transition. Such a shape transition was observed e.g., by Hines et al.<sup>33</sup> The astonishing luminescence enhancement in air for our PbS NCs and size regime, contradicting other studies of photobrightening and photodarkening of PbS NCs where irreversible oxidation-induced luminescence quenching was observed,<sup>76</sup> suggests a passivation of surface defects by this surface oxidation. In addition, the efficiency of the “intrinsic” nonradiative interband recombination caused by the increase in bandgap in oxidized, i.e., smaller PbS NC, could be also reduced.<sup>43</sup>

Our explanation for the aging-induced luminescence enhancement is supported by the improved stability of 4.4 nm PbS NCs kept under inert gas. This is reflected by only very small time-dependent changes in the spectral position of the emission maximum located

at 1390 nm, matching the initial value found for the freshly synthesized 4.4 nm PbS NC in the presence of oxygen (Figure 5, upper panel), and its considerably smaller  $\Phi_f$  of 0.15.

<Insert Figure 5 here>

*Photostability and  $\Phi_f$  of PbS.* Within the context of the desired validation of absolute measurements of photoluminescence with our new integrating sphere setup, we measured the  $\Phi_f$  of aged PbS NC colloids (4.4 nm PbS NCs stored both in air and under inert gas) at different excitation wavelengths relatively and absolutely with different excitation radiant powers. Relative measurements with excitation radiant powers of 0.1 mW in the wavelength region of 690 nm to 915 nm (see *SI*, Figure 2S), revealed no or only very small light-induced changes in absorption and emission as well as excitation wavelength-independent  $\Phi_f$ . Absolute fluorescence measurements with the exemplarily chosen more intense 808 nm laser, however, revealed radiant power-dependent photoeffects for all three PbS NCs, which affect resulting  $\Phi_f$  values. This is exemplarily shown for 4.4 nm PbS NCs aged in air for *ca.* 300 days (Figure 5, middle panel, right) and stored under inert gas atmosphere (Figure 5, middle panel, left). For 4.4 nm PbS in air,  $\Phi_f$  decreased at short illumination times and subsequently increased again, reaching almost the starting  $\Phi_f$  value. Simultaneously, its absorption and emission are blue shifted by *ca.* 10 nm (Figure 5, lower panels, blue spectra), indicative of slight photocorrosion. Similar photoeffects, i.e., photobrightening and photodarkening, commonly ascribed to (reversible) trapping of carriers to a long-lived, optically dark state or particle charging, have been already reported for PbS quantum dots.<sup>76</sup> Illumination of 4.4 nm PbS NCs in the absence of

oxygen leads to a blue shift in absorption and especially in emission by about 50 nm (Figure 5, lower panels, black spectra) and an increase in  $\Phi_f$  by a factor of almost two (Figure 5, middle panel, left). The eventually reached  $\Phi_f$  of 0.27 is, however, still clearly smaller than the  $\Phi_f$  of 0.45 obtained for the same PbS colloid in air (Figure 5, upper panel). Purging of the solution of the air-aged PbS NCs with argon did not alter the light-induced spectroscopic changes revealed by this colloid, still showing photodarkening followed by photobrightening upon light exposure. Apparently, aging in air changed the NC surface chemistry irreversibly, which confirms the the formation of a  $\text{PbSO}_x$  layer at the NC surface as reported e.g., by Tang et al.<sup>74</sup> and Hardman et al..<sup>75</sup>

Similar experiments with 2.3 nm and 4.1 nm PbS NCs in air (see *SI*, Figure 12S) revealed size-dependent photoeffects. The smallest PbS colloid showed solely photobrightening, leading to an increase of the initially obtained  $\Phi_f$  of 0.18 to 0.71, respectively, accompanied by a blue shift of the emission band from 958 nm to 920 nm. At lower radiant powers, also fast photodarkening was observed, yet in all cases, subsequent photobrightening dominated, always yielding similarly high  $\Phi_f$ . Contrary, 4.1 nm PbS NCs showed a similar behavior as 4.4 nm PbS particles and comparable  $\Phi_f$ . These size-dependent differences in photochemical behavior seem to correlate with the size-dependent aging of these colloids, providing a further hint for a different surface chemistry of our three PbS NCs.

*Comparison of absolute and relative  $\Phi_f$  measurements for PbS.* As exemplarily shown for our 4.4 nm PbS colloid in air and under inert gas atmosphere, principally, the absolutely measured initial  $\Phi_f$  values agree reasonably well with relatively obtained data (see e.g., Figure 5; finally reached  $\Phi_f$  after 300 days in top panel and starting  $\Phi_f$  value in

the middle right panel for PbS in air and for PbS under inert gas, initial  $\Phi_f$  after synthesis from top panel and starting  $\Phi_f$  value in the middle left panel, respectively). The desired comparison of relatively and absolutely measured  $\Phi_f$  data for PbS is, however, hampered by the radiant power- and size-dependent photodarkening and photobrightening of this material, since these measurements are commonly performed at different excitation radiant powers (see *SI*). Our results are nevertheless very interesting for a better understanding of the factors yielding very bright PbS NC. In this respect, it should be kept in mind that the measurement conditions used by us for the absolute determination of  $\Phi_f$  of the PbS NCs most likely closely mimic those of absolute measurements reported by other groups in the IR wavelength region. Integrating sphere measurements with IR-emissive NCs like lead chalcogenides are commonly performed with intense excitation light sources like a 831 nm semiconductor laser,<sup>67, 68, 77</sup> LEDs emitting at 850 nm or 950 nm,<sup>43</sup> or a 405 nm laser,<sup>78</sup> respectively, with no information provided on excitation radiant powers employed. There are only very few reports of integrating sphere setups for measurements > 1000 nm using a fiber coupled xenon lamp-monochromator ensemble as less intense excitation light source.<sup>79</sup> Hence, measurement condition- and material-specific photo-induced changes in fluorescence intensity as found by us for PbS NCs could principally also affect other literature data, especially in the case of potentially oxygen- and light-sensitive lead chalcogenides.

#### 4 Conclusions and Outlook

In summary, we presented the design of a new integrating sphere setup for spectrally resolved measurements of absolute photoluminescence quantum yields ( $\Phi_f$ ) of barely to

moderately emissive organic dyes to highly emissive semiconductor NCs in the wavelength region of 600 – 1600 nm and addressed common instrument- and material-related challenges for fluorescence measurements in the NIR and IR and solutions. We demonstrated the reliability of our measurements by comparing the corrected emission spectra and relatively and absolutely determined  $\Phi_f$  of several organic dyes, MPA-capped  $\text{Cd}_{1-x}\text{Hg}_x\text{Te}$  in  $\text{D}_2\text{O}$ , and oleate-capped PbS NCs in TCE obtained with two integrating sphere setups and a spectrofluorometer, all independently calibrated. These validation strategies provide a good example for the validation of challenging fluorescence measurements in the NIR and IR for e.g., semiconductor quantum dots and rods, carbon nanotubes, and upconversion materials.

Moreover, we redetermined the  $\Phi_f$  of the only IR reference dye IR26 to  $1.1 \times 10^{-3}$  with an uncertainty of  $2.3 \times 10^{-4}$  derived from an uncertainty budget and introduced a procedure for the simultaneous correction for sample reabsorption and solvent absorption. These effects present common signal distortions in the IR. A further reduction in measurement uncertainties requires especially an improved stability of the excitation light sources used for our NIR/IR integrating sphere setup. We could verify the high  $\Phi_f$  of 0.3 to 0.7 for high quality aqueous  $\text{Cd}_{1-x}\text{Hg}_x\text{Te}$  NC colloids prepared via our previously reported simple one pot synthesis. For differently sized oleate-capped PbS colloids with  $\Phi_f$  between of 0.2 to 0.7, we demonstrated the influence of quantum dot-inherent photobrightening and photodarkening on  $\Phi_f$  measurements, which can be material-specific, size-dependent, and affected by oxygen. These effects, which can be expected also e.g., for other lead chalcogenides, together with the considerable overassessment of many previously published  $\Phi_f$  of NIR- and IR-emissive quantum dots like PbS, PbSe, and

$\text{Cd}_{1-x}\text{Hg}_x\text{Te}$  derived from our reexamined  $\Phi_f$  of the reference dye IR26 underline the need for a critical reevaluation of  $\Phi_f$  values of IR-emissive nanomaterials. A critical evaluation of  $\Phi_f$  data and procedures used for the determination of  $\Phi_f$  is generally of considerable importance with respect to the foreseeable increasing importance of luminescence measurements in the wavelength region of 1000 – 1600 nm e.g., for bioimaging studies. This similarly triggers the need for broadly available and well characterized quantum yield standards also for this wavelength region.

**Acknowledgement.** We express our gratitude to Dr. Markus Grabolle (BAM) for many fruitful discussions, to Dipl.-Ing A. Güttler for technical assistance during the calibration of the spectrofluorometer FSP920, and to Frau M. Spieles (BAM) for the HPLC measurements of the dyes. We gratefully acknowledge financial support from the Deutsche Forschungsgemeinschaft (DFG grant RE-1203/12-1 and EY 16/14-1).



## Figure and Table Captions

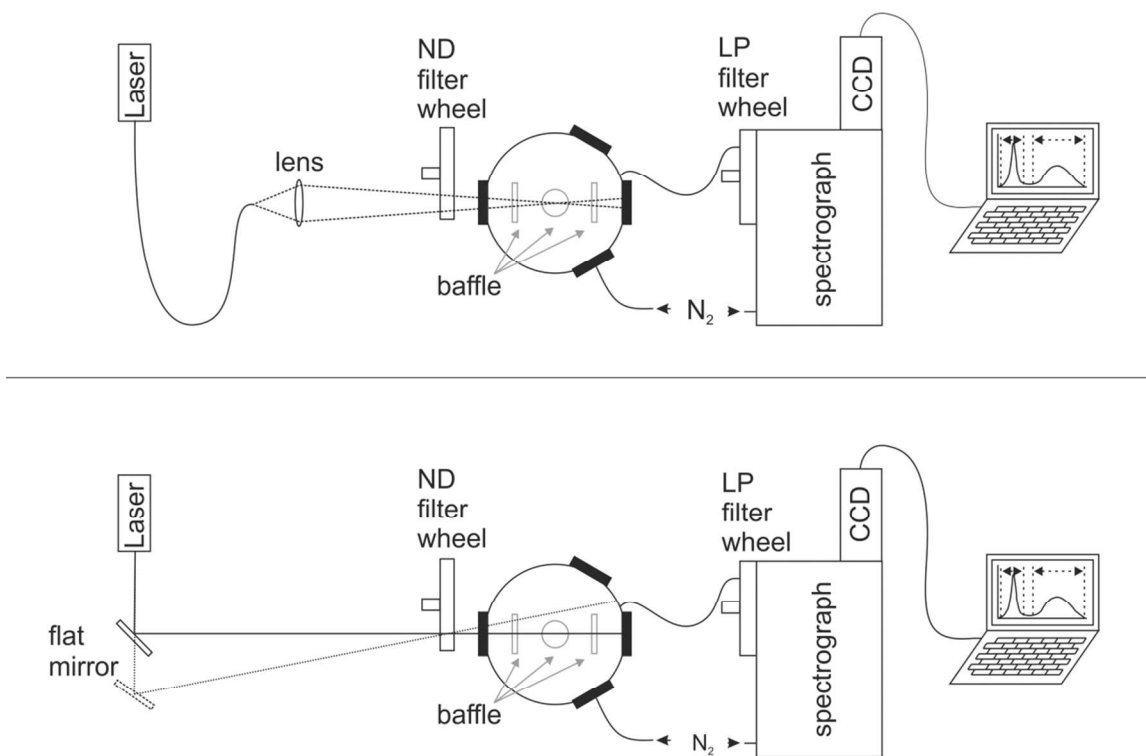


**Figure 1.** NIR/IR Integrating sphere setup for absolute measurement of photoluminescence in the wavelength region of 600 nm to 1600 nm consisting of several high stability (intensity fluctuations < 1 %) lasers and laser diodes, coupled either via fiber optics (upper panel; 808 and 980 nm laser diodes) or directly (HeNe laser, 690 nm, 730 nm, and 785 nm laser diodes; 914 nm solid-state laser) with a flat mirror (lower panel) to a N<sub>2</sub>-purged 12 cm integrating sphere attached via a IR-quartz fiber bundle to an imaging spectrograph equipped with a InGaAs CCD. The mirrors can be used for direct or indirect sample illumination. Two filter wheels, one equipped with neutral density (ND) filters placed between the sphere and the light sources, and one equipped

with different long pass (LP) interference filters (cut-on wavelengths of 600, 800, 950, and 1000 nm) in front of the detection system, enable control of the exciting radiant power and remove second order diffractions. Dye solutions and NC dispersions in cuvettes are placed in the center of the sphere using a custom designed Spectrafect-coated cell holder.

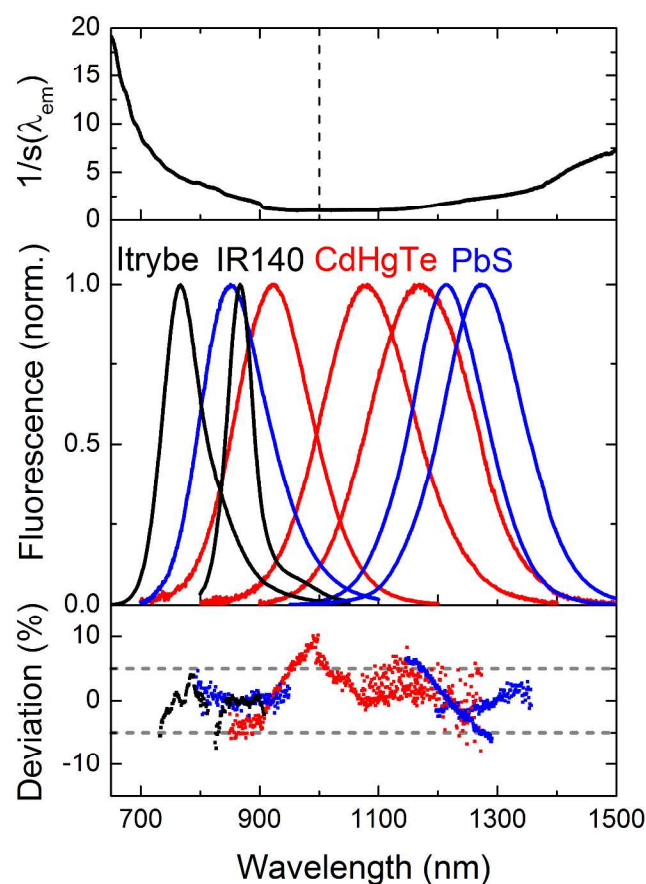


**Figure 2.** Top: Inverse spectral responsivity  $1/s(\lambda_{em})$  of the NIR/IR integrating sphere setup determined with two calibration lamps. Middle: Normalized corrected emission spectra of the NIR dyes Itrybe (solvent ethanol; black line) and IR140 (solvent DMSO; black line), MPA-stabilized CdHgTe NC colloids of various composition and size dispersed in air-saturated  $D_2O$  (red lines), and

PbS colloids of various size in TCE (blue lines) in air obtained with our NIR/IR integrating sphere setup. Bottom: Relative spectral deviations between the corrected spectra measured with the integrating sphere setup and an independently calibrated spectrofluorometer (data given for intensities up to 50 % of the intensity at the respective emission maximum). The dotted grey lines indicated relative deviations of 5 %.

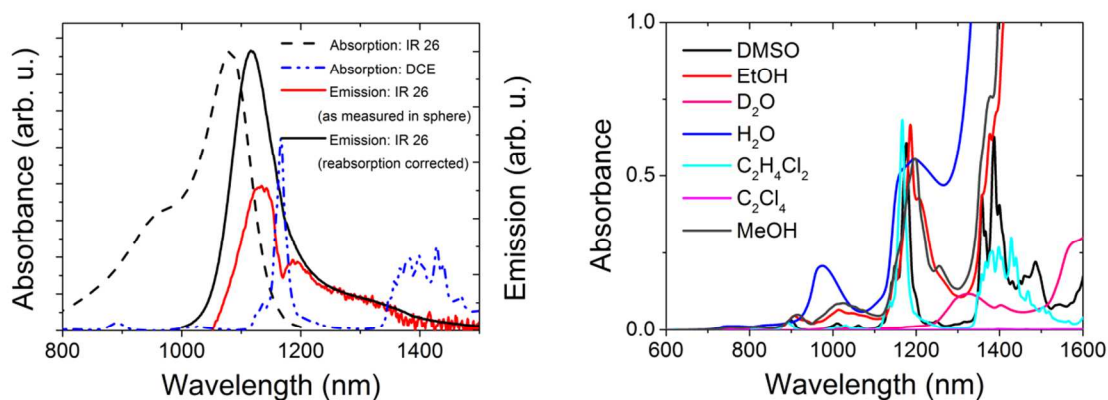


**Figure 3.** Left: Normalized absorption and emission spectra of IR26 in DCE (without and with correction for dye reabsorption solvent absorption) and absorption of the solvent DCE within the wavelength region of dye emission. Right: Absorption spectra of common organic solvents, H<sub>2</sub>O, and D<sub>2</sub>O used for the study of IR dyes and NCs, given for an optical path length of 1 cm.

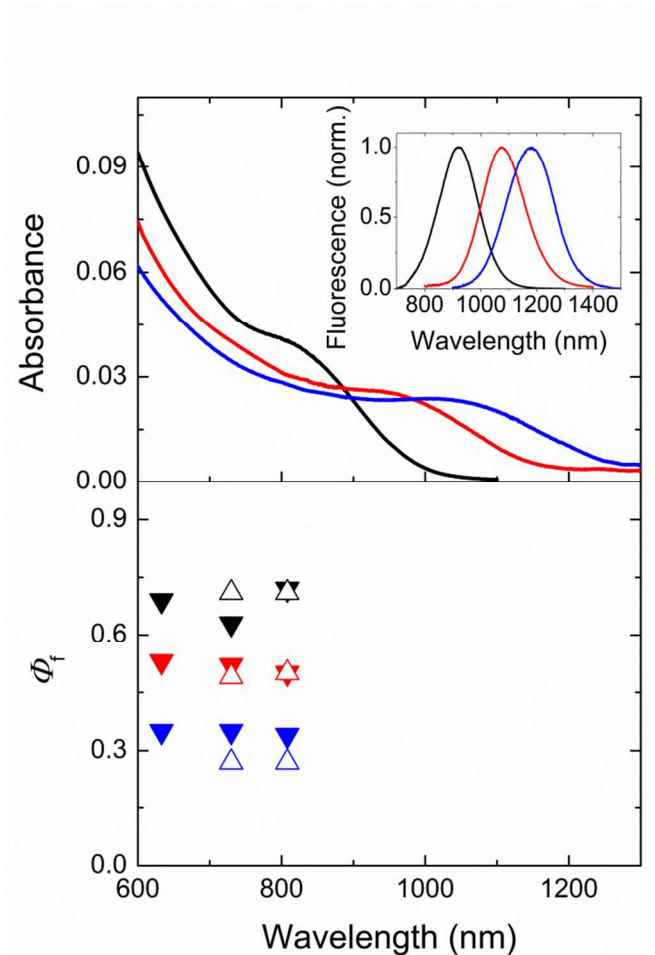


**Figure 4.** Top: Normalized absorption spectra of three representative Cd<sub>1-x</sub>Hg<sub>x</sub>Te NC colloids of different size and composition (black: 4.2. nm, Cd:Hg = 99:1, concentration (c) = 1.3×10<sup>-6</sup> mol/L; red: 6.3 nm, Cd:Hg = 98:2, c = 1.3×10<sup>-6</sup> mol/L; blue: 7.1 nm, Cd:Hg = 97:3, c = 5.2×10<sup>-7</sup> mol/L) in D<sub>2</sub>O in air. The corresponding corrected emission spectra are shown in the inset and in Figure 2 (middle panel). The concentration of the Cd<sub>1-x</sub>Hg<sub>x</sub>Te NC was determined by measuring the concentration of the respective metal ions (Cd<sup>2+</sup> and Hg<sup>2+</sup>) via ICP-OES as previously described<sup>15, 73</sup> and considering the NC diameter derived from TEM data. Bottom: Absolutely measured Φ<sub>f</sub> (solid symbols) and

relatively measured  $\Phi_f$  (open symbols) at different excitation wavelengths. Considering the uncertainties of both methods determined values overlap.

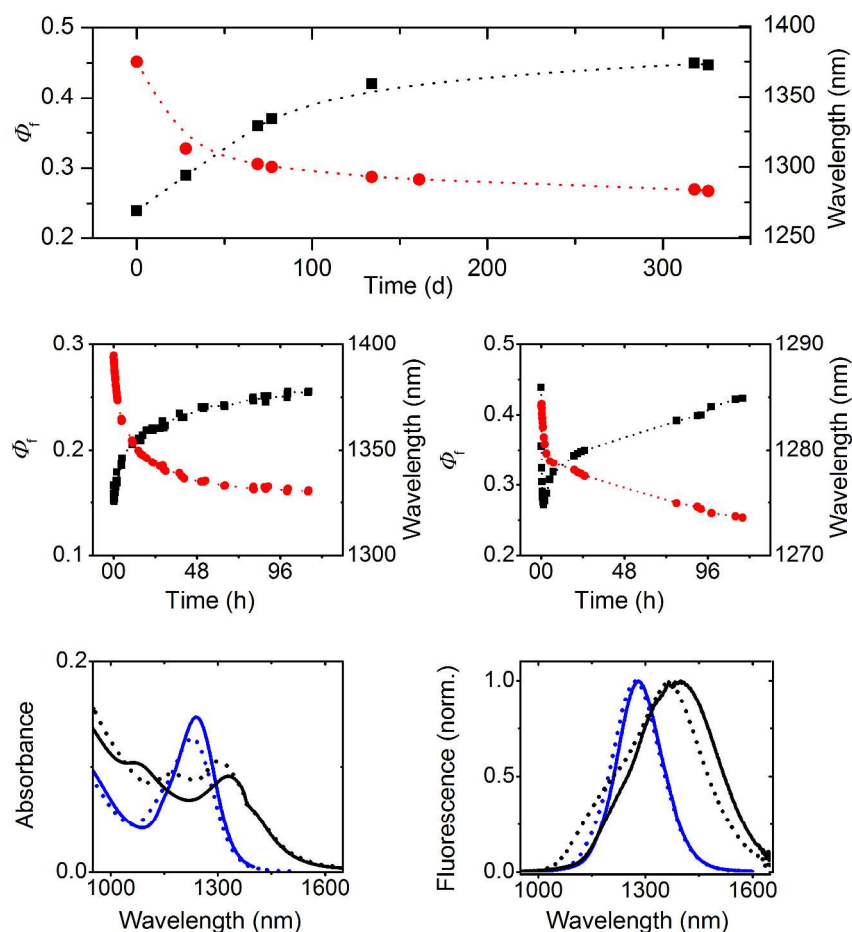


**Figure 5.** Top: Aging of 4.4 nm PbS NCs in air. Blue shift of the spectral position of the emission band (red circles) and in the relatively measured  $\Phi_f$  (black squares) of 4.4 nm PbS NCs as a function of time after colloid preparation. Middle: Absolutely measured  $\Phi_f$  and photoeffects. Change in absolutely measured  $\Phi_f$  (black squares) and in the spectral position of the emission band (red circles) of 4.4 nm PbS NCs kept under inert gas (left panel) and of 4.4 nm PbS NCs, both aged in air for ca. 300 days, as a function of illumination time.

Illumination was performed with the 808 nm laser diode of the integrating sphere setup (radiant power of 62 mW). Bottom: Aging and light-induced spectral changes. Change in the absorption spectra (left panel) of 4.4 nm PbS NCs aged/stored under inert gas for *ca.* 300 days (black) and in air (blue) and diluted with TCE, before (solid lines) and after illumination (dashed lines) with the 808 nm laser diode of the integrating sphere setup (radiant power of 62 mW) for 120 hours. The initial absorption spectrum of 4.4 nm PbS NCs stored under inert gas atmosphere (black solid line) closely matches the initial absorption spectrum of this colloid prior to aging in air (top panel).

**Table 1.** Comparative absolute and relative measurements of  $\Phi_f$  of the organic dyes Itrybe ( $\lambda_{\text{ex}} = 633$  nm; relative to HITCI in ethanol,  $\Phi_f = 0.30$ ) and IR140 ( $\lambda_{\text{ex}} = 808$  nm; relative to IR125 in DMSO,  $\Phi_f = 0.23$ ) emitting < 1000 nm (Figure 1) and IR26 ( $\lambda_{\text{ex}} = 980$  nm; relative to IR125 in DMSO excited at 808 nm using a previously controlled excitation correction) emitting > 1000 nm (Figure 3, left panel); absolute 1: NIR/IR integrating sphere setup, absolute 2: UV/vis/NIR integrating sphere setup; relative: fluorometer FSP 920.

Dye	Solvent	$\Phi_f$ Absolute <sup>1</sup>	$\Phi_f$ Absolute <sup>2</sup>	$\Phi_f$ Relative	$\Phi_f$ Lit
Itrybe	EtOH	0.22		0.23	-
IR140	DMSO	0.20	0.20	0.20	-
IR26	DCE	0.0011	-	0.0007	0.00048

## References

1. B. Valeur, *Molecular Fluorescence: Principles and Application*, Wiley-VCH, Weinheim, 2002.
2. D. M. Jameson, J. C. Croney and P. D. J. Moens, *Biophotonics, Pt A*, 2003, 360, 1-43.
3. S. V. Kershaw, A. S. Sussha and A. L. Rogach, *Chemical Society Reviews*, 2013, 42, 3033-3087.
4. M. T. Harrison, S. V. Kershaw, M. G. Burt, A. L. Rogach, A. Kornowski, A. Eychmuller and H. Weller, *Pure and Applied Chemistry*, 2000, 72, 295-307.
5. P. V. Kamat, *The Journal of Physical Chemistry C*, 2008, 112, 18737-18753.
6. E. H. Sargent, *Advanced Materials*, 2005, 17, 515-522.
7. M. Graetzel, R. A. J. Janssen, D. B. Mitzi and E. H. Sargent, *Nature*, 2012, 488, 304-312.
8. U. Resch-Genger, M. Grabolle, S. Cavaliere-Jaricot, R. Nitschke and T. Nann, *Nature Methods*, 2008, 5, 763-775.
9. C. Würth, M. Grabolle, J. Pauli, M. Spieles and U. Resch-Genger, *Nature Protocols*, 2013, 8, 1535-1550.
10. S. E. Braslavsky, *Pure and Applied Chemistry*, 2007, 79, 293-465.
11. U. Resch-Genger and K. Rurack, *Pure and Applied Chemistry*, 2013, 85, 2005-2026.
12. C. T. Xu, Q. Q. Zhan, H. C. Liu, G. Somesfalean, J. Qian, S. L. He and S. Andersson-Engels, *Laser & Photonics Reviews*, 2013, 7, 663-697.
13. S. L. Gai, C. X. Li, P. P. Yang and J. Lin, *Chemical Reviews*, 2014, 114, 2343-2389.
14. M. Grabolle, M. Spieles, V. Lesnyak, N. Gaponik, A. Eychmuller and U. Resch-Genger, *Analytical Chemistry*, 2009, 81, 6285-6294.
15. S. Leubner, S. Hatami, N. Esendemir, T. Lorenz, J. O. Joswig, V. Lesnyak, S. Recknagel, N. Gaponik, U. Resch-Genger and A. Eychmuller, *Dalton Transactions*, 2013, 42, 12733-12740.
16. J. C. Boyer, M. P. Manseau, J. I. Murray and F. van Veggel, *Langmuir*, 2010, 26, 1157-1164.
17. F. Wang, J. A. Wang and X. G. Liu, *Angewandte Chemie-International Edition*, 2010, 49, 7456-7460.
18. J. Ziegler, A. Merkulov, M. Grabolle, U. Resch-Genger and T. Nann, *Langmuir*, 2007, 23, 7751-7759.
19. L. H. Qu and X. G. Peng, *Journal of the American Chemical Society*, 2002, 124, 2049-2055.
20. J. B. Delehanty, K. Susumu, R. L. Manthe, W. R. Algar and I. L. Medintz, *Analytica Chimica Acta*, 2012, 750, 63-81.
21. X. H. Ji, D. Copenhaver, C. Sichmeller and X. G. Peng, *Journal of the American Chemical Society*, 2008, 130, 5726-5735.
22. G. Kalyuzhny and R. W. Murray, *Journal of Physical Chemistry B*, 2005, 109, 7012-7021.
23. C. Wang, X. Gao and X. Su, *Analytical and Bioanalytical Chemistry*, 2010, 397, 1397-1415.

24. C. Würth, M. Grabolle, J. Pauli, M. Spieles and U. Resch-Genger, *Analytical Chemistry*, 2011, 83, 3431–3439.
25. C. Würth, J. Pauli, C. Lochmann, M. Spieles and U. Resch-Genger, *Analytical Chemistry*, 2012, 84, 1345-1352.
26. C. Würth, M. G. Gonzalez, R. Niessner, U. Panne, C. Haisch and U. R. Genger, *Talanta*, 2012, 90, 30-37.
27. K. Suzuki, A. Kobayashi, S. Kaneko, K. Takehira, T. Yoshihara, H. Ishida, Y. Shiina, S. Oishi and S. Tobita, *Phys Chem Chem Phys*, 2009, 11, 9850-9860.
28. K. Rurack, in *Standardization and Quality Assurance in Fluorescence Measurements I: Techniques*, ed. U. Resch-Genger, Springer, Berlin-Heidelberg, 2008, vol. 5.
29. D. F. Eaton, *Pure and Applied Chemistry*, 1988, 60, 1107-1114.
30. A. M. Brouwer, *Pure and Applied Chemistry*, 2011, 83, 2213-2228.
31. J. R. Lakowicz, *Principles of fluorescence spectroscopy*, Springer Science+Business Media, LLC, New York, 3rd edn., 2006.
32. J. N. Demas and G. A. Crosby, *Journal of Physical Chemistry*, 1971, 75, 991-1024.
33. M. A. Hines and G. D. Scholes, *Advanced Materials*, 2003, 15, 1844-1849.
34. H. Du, C. L. Chen, R. Krishnan, T. D. Krauss, J. M. Harbold, F. W. Wise, M. G. Thomas and J. Silcox, *Nano Letters*, 2002, 2, 1321-1324.
35. L. Cademartiri, J. Bertolotti, R. Sapienza, D. S. Wiersma, G. von Freymann and G. A. Ozin, *Journal of Physical Chemistry B*, 2006, 110, 671-673.
36. J. J. Peterson and T. D. Krauss, *Nano Letters*, 2006, 6, 510-514.
37. F. Q. Ren, H. G. Zhao, F. Vetrone and D. L. Ma, *Nanoscale*, 2013, 5, 7800-7804.
38. R. C. Benson and H. A. Kues, *Physics in Medicine and Biology*, 1978, 23, 159-163.
39. J. E. Murphy, M. C. Beard, A. G. Norman, S. P. Ahrenkiel, J. C. Johnson, P. R. Yu, O. I. Micic, R. J. Ellingson and A. J. Nozik, *Journal of the American Chemical Society*, 2006, 128, 3241-3247.
40. B. L. Wehrenberg, C. J. Wang and P. Guyot-Sionnest, *Journal of Physical Chemistry B*, 2002, 106, 10634-10640.
41. M. V. Kovalenko, R. D. Schaller, D. Jarzab, M. A. Loi and D. V. Talapin, *Journal of the American Chemical Society*, 2012, 134, 2457-2460.
42. V. Lesnyak, A. Lutich, N. Gaponik, M. Grabolle, A. Plotnikov, U. Resch-Genger and A. Eychmuller, *Journal of Materials Chemistry*, 2009, 19, 9147-9152.
43. O. E. Semonin, J. C. Johnson, J. M. Luther, A. G. Midgett, A. J. Nozik and M. C. Beard, *Journal of Physical Chemistry Letters*, 2010, 1, 2445-2450.
44. W. Kranitzky, B. Kopainsky, W. Kaiser, K. H. Drexhage and G. A. Reynolds, *Optics Communications*, 1981, 36, 149-152.
45. B. Kopainsky, P. Qiu, W. Kaiser, B. Sens and K. H. Drexhage, *Applied Physics B-Photophysics and Laser Chemistry*, 1982, 29, 15-18.
46. U. Resch-Genger and P. C. DeRose, *Pure Applied Chemistry* 2012, 84, 1815-1835.
47. C. Würth, C. Lochmann, M. Spieles, J. Pauli, K. Hoffmann, T. Schuttrigkeit, T. Franzl and U. Resch-Genger, *Applied Spectroscopy*, 2010, 64, 733-741.



48. S. H. Xu, C. L. Wang, Q. Y. Xu, R. Q. Li, H. B. Shao, H. S. Zhang, M. Fang, W. Lei and Y. P. Cui, *Journal of Physical Chemistry C*, 2010, 114, 14319-14326.
49. T. V. Duncan, M. A. M. Polanco, Y. Kim and S. J. Park, *Journal of Physical Chemistry C*, 2009, 113, 7561-7566.
50. D. Tonti, F. van Mourik and M. Chergui, *Nano Letters*, 2004, 4, 2483-2487.
51. R. A. Cruz, V. Pilla and T. Catunda, *Journal of Applied Physics*, 2010, 107.
52. Z. M. Tao, G. S. Hong, C. Shinji, C. X. Chen, S. Diao, A. L. Antaris, B. Zhang, Y. P. Zou and H. J. Dai, *Angewandte Chemie-International Edition*, 2013, 52, 13002-13006.
53. G. Hong, S. Diao, J. Chang, A. L. Antaris, C. Chen, B. Zhang, S. Zhao, D. N. Atochin, P. L. Huang, K. I. Andreasson, C. J. Kuo and H. Dai, *Nat Photon*, 2014, 8, 723-730.
54. D. Salo, H. R. Zhang, D. M. Kim and M. Y. Berezin, *Journal of Biomedical Optics*, 2014, 19.
55. V. Lesnyak, N. Gaponik and A. Eychmueller, *Chemical Society Reviews*, 2013, 42, 2905-2929.
56. S. Gupta, O. Zhovtiuk, A. Vaneski, Y.-C. Lin, W.-C. Chou, S. V. Kershaw and A. L. Rogach, *Particle & Particle Systems Characterization*, 2013, 30, 346-354.
57. E. H. Sargent, *Nature Photonics*, 2012, 6, 133-135.
58. J. Poppe, S. Gabriel, L. Liebscher, S. G. Hickey and A. Eychmueller, *Journal of Materials Chemistry C*, 2013, 1, 1515-1524.
59. L. Cademartiri, E. Montanari, G. Calestani, A. Migliori, A. Guagliardi and G. A. Ozin, *Journal of the American Chemical Society*, 2006, 128, 10337-10346.
60. P. C. DeRose and U. Resch-Genger, *Analytical Chemistry*, 2010, 82, 2129-2133.
61. U. Resch-Genger, D. Pfeifer, C. Monte, W. Pilz, A. Hoffmann, M. Spieles, K. Rurack, J. Hollandt, D. Taubert, B. Schonenberger and P. Nording, *Journal of Fluorescence*, 2005, 15, 315-336.
62. J. C. de Mello, H. F. Wittmann and R. H. Friend, *Advanced Materials*, 1997, 9, 230-232.
63. U. Resch-Genger, W. Bremser, D. Pfeifer, M. Spieles, A. Hoffmann, P. C. DeRose, J. C. Zwinkels, F. o. Gauthier, B. Ebert, R. D. Taubert, C. Monte, J. Voigt, J. Hollandt and R. Macdonald, *Analytical Chemistry*, 2012, 84, 3889-3898.
64. T. Behnke, J. E. Mathejczyk, R. Brehm, C. Wurth, F. R. Gomes, C. Dullin, J. Napp, F. Alves and U. Resch-Genger, *Biomaterials*, 2013, 34, 160-170.
65. D. Brown and D. Benfey, *Comprehensive Study of Diode-Pumped Dye Lasers. Phase 1*, 1991.
66. S. Hinds, S. Myrskog, L. Levina, G. Koleilat, J. Yang, S. O. Kelley and E. H. Sargent, *Journal of the American Chemical Society*, 2007, 129, 7218-+.
67. L. Bakueva, I. Gorelikov, S. Musikhin, X. S. Zhao, E. H. Sargent and E. Kumacheva, *Advanced Materials*, 2004, 16, 926-929.
68. X. S. Zhao, I. Gorelikov, S. Musikhin, S. Cauchi, V. Sukhovatkin, E. H. Sargent and E. Kumacheva, *Langmuir*, 2005, 21, 1086-1090.
69. M. Sykora, A. Y. Kuposov, J. A. McGuire, R. K. Schulze, O. Tretiak, J. M. Pietryga and V. I. Klimov, *Acs Nano*, 2010, 4, 2021-2034.
70. J. W. Stouwdam, J. Shan, F. van Veggel, A. G. Pattantyus-Abraham, J. F. Young and M. Raudsepp, *Journal of Physical Chemistry C*, 2007, 111, 1086-1092.

71. I. Moreels, Y. Justo, B. De Geyter, K. Haustraete, J. C. Martins and Z. Hens, *Acs Nano*, 2011, 5, 2004-2012.
72. H. Choi, J.-H. Ko, Y.-H. Kim and S. Jeong, *Journal of the American Chemical Society*, 2013, 135, 5278-5281.
73. S. Leubner, R. Schneider, A. Dubavik, S. Hatami, N. Gaponik, U. Resch-Genger and A. Eychmuller, *Journal of Materials Chemistry C*, 2014, 2, 5011-5018.
74. J. Tang, L. Brzozowski, D. A. R. Barkhouse, X. Wang, R. Debnath, R. Wolowiec, E. Palmiano, L. Levina, A. G. Pattantyus-Abraham, D. Jamakosmanovic and E. H. Sargent, *ACS Nano*, 2010, 4, 869-878.
75. S. J. O. Hardman, D. M. Graham, S. K. Stubbs, B. F. Spencer, E. A. Seddon, H.-T. Fung, S. Gardonio, F. Sirotti, M. G. Silly, J. Akhtar, P. O'Brien, D. J. Binks and W. R. Flavell, *Physical Chemistry Chemical Physics*, 2011, 13, 20275-20283.
76. J. J. Peterson and T. D. Krauss, *Physical Chemistry Chemical Physics*, 2006, 8, 3851-3856.
77. T. W. F. Chang, A. Maria, P. W. Cyr, V. Sukhovatkin, L. Levina and E. H. Sargent, *Synthetic Metals*, 2005, 148, 257-261.
78. J. S. Steckel, S. Coe-Sullivan, V. Bulovic and M. G. Bawendi, *Advanced Materials*, 2003, 15, 1862-1866.
79. E. Lifshitz, M. Brumer, A. Kigel, A. Sashchiuk, M. Bashouti, M. Sirota, E. Galun, Z. Burshtein, A. Q. Le Quang, I. Ledoux-Rak and J. Zyss, *Journal of Physical Chemistry B*, 2006, 110, 25356-25365.